J Mater Sci: Mater Med (2008) 19:1871–1879
DOI 10.1007/s10856-007-3264-6

# Thin films of $SiO_2$ and hydroxyapatite on titanium deposited by spray pyrolysis

**V. Jokanovic · B. Jokanovic · D. Izvonar · B. Dacic**

Received: 30 June 2006 / Accepted: 14 August 2007 / Published online: 4 October 2007
© Springer Science+Business Media, LLC 2007

**Abstract** Wet spray pyrolysis of fine, well-dispersed a $SiO_2$ sol was used for the deposition of thin films of silicon dioxide. The sol was obtained by hydrothermal precipitation of silicon acid from a solution at pH = 10. The morphology, roughness, phase composition, chemical homogeneity and the mechanism of the films were investigated by SEM, EDS and IR spectroscopy. The obtained results show a complete covering of the titanium substrate with $SiO_2$ after 3 h of deposition. It was observed that the film thickness increased from 3 to 19 µm, the roughness of the film decreased from 12 to 3 µm, while the morphology of the deposit changed considerably. A hydroxyapatite film was prepared on the so-obtained $SiO_2$ thin film by spray pyrolysis deposition and its morphology and phase composition were investigated.

V. Jokanovic (✉)
Institute of Nuclear Sciences "Vinča" Laboratory for Radiation Chemistry and Physics, P.O. Box 522, Belgrade 11001, Republic of Serbia
e-mail: vukomanj@ptt.yu

B. Jokanovic
Institut fur Metallurgie, Termochemie und Mikrokinetik, Technische Universität Clausthal, Clausthal-Zellerfeld, Germany

D. Izvonar
Faculty of Applied Arts, Belgrade, Republic of Serbia

B. Dacic
Plasma Jet Co. – Titanox Development Ltd, Auckland, New Zealand

## 1 Introduction

Spray pyrolysis with ultrasound excitation is one of the most promising methods for the deposition of thin films with well-defined phase composition and chemical homogeneity. The principle advantage, beside its simplicity, is that each single drop of aerosol is itself a separate system, which posses all the characteristics of the system as a whole—its chemistry and phase composition [1–10]. There are numerous other methods for the deposition of thin films, such as CVD methods assisted with different types of plasmas (microwave, radio frequency, laser induced and thermal plasma), reactive cathode vacuum arc deposition, deposition stimulated by electron-beam evaporation, reactive magnetron sputtering, electrophoretic deposition and others [11–17]. In addition to the advantages which some of these methods have regarding increased adhesion of the deposited films and greater smoothness (CVD deposition), spray pyrolysis counts to one of the most convenient methods of deposition on substrates very diverse in shape and form. The cost of the method is significantly lower and the method is applicable for very diverse substrate/film systems, while the films have excellent chemical and phase homogeneity [1–10].

Spray pyrolysis with ultrasound excitation can be used twofold, i.e., (i) as a deposition method by wetting the substrate surface with aerosol droplets of defined size and chemical composition and (ii) as a method for the production of powders with well-defined size, shape and inner sub-structure, which are then self-assembled on the substrate surface by a slow deposition process [8, 18, 19].

In this study, the method of homogeneous wetting of a titanium substrate with droplets of a $SiO_2$ sol with a well-defined size distribution was employed, which proceeded thermal treatment, leading to the solidification of the

deposit into a thin film. The thickness, morphology and roughness of the film were dependent primarily on the deposition time. The mechanism of deposition changed as it progressed.

Deposition of $SiO_2$ on titanium surface is of primary importance for a better biocompatibility of titanium implants in medicine such as dental implants and implants in maxi facial and oral surgery. Very often this film is used as an interlayer on a titanium substrate on which a calcium hydroxyapatite coating comes, because the coefficient of thermal expansion for $SiO_2$ is closer to that of titanium and, therefore, the mechanical strain between calcium hydroxyapatite and the substrate is improved and, in that way, the functional property of the system as a whole. Also, because of its own good compatibility with living tissues, $SiO_2$ in contact with the flesh fluids allows hydroxyapatite of biological origin to deposit on its own surface [20–25].

One of probably the most important applications of $SiO_2$ thin films is in medicine for coating metal implants based on titanium alloys, which have excellent mechanical properties and corrosion stability, but have insufficient bio-compatibility. Therefore, the coating of titanium implants with ceramics offers a bio-engineering approach to solve this problem via the formation of hydroxyapatite thin films or, in some cases, bio-apatite in situ on the surface of $SiO_2$ films. Such apatite has excellent osteo-conductivity, what makes them the material of choice for osteo-integrative and functional properties [20–28].

## 2 Experiments

### 2.1 Preparation of the precursor

The silicon dioxide sol was synthesized through the following successive processes: (i) hydrothermal leaching of liquid glass; (ii) hydrothermal peptization of the silica acid precipitate and adjustment of the concentration of the obtained colloidal solution to 2 M by dilution with deionized water.

The leached precursor was $Na_2O_3SiO_2$ (water glass) with a silicate module ($SiO_2/Na_2O$) of 3.75 and viscosity of 2.2 Poaza. The leaching was conducted by slow peptization (drop wise addition of 0.1 M HCl) with vigorous mixing of the solution at a temperature of 80 °C. The total amount of acid consumed for the leaching corresponded exactly to the stoichiometry ratio required for complete neutralization of the treated amount of water glass. The ratio of liquid to solid (water:water glass) was 4:1 at the start of the leaching. After addition of the amount of 0.1 M HCl required for leaching, the mixture was transferred to an autoclave, where the leaching was continued for 5 h at a temperature of 120 °C under a pressure of 3 bars.

The obtained precipitate was separated from the solution by centrifugation at 10,000 revolutions/min. Then, deionized water was added and the ratio of liquid: solid phase was again adjusted to 4:1 and 0.1 M HCl (20% of the amount employed in the previously step) was added. The mixture was returned to the autoclave for additional leaching. At the end of the second stage of leaching, the precipitate was separated by centrifugation, rinsed with hot de-ionize water and decanted.

The 20 g of deposit precipitated from the previous treatment were diluted with 200 mL de-ionized water, the alkalinity of which had been adjusted to pH = 10 with 0.1 N NaOH. This mixture was then heated at 80°C and the alkalinity of solution again adjusted to pH 10 with 0.1 N NaOH accompanied under vigorous stirring. The mixture was then transferred to an autoclave where peptization occurred during 8 h at a temperature of 120 °C at a pressure of 3 bars. At the end of the hydrothermal treatment, the pH of the obtained sol was 9 and the concentration of $SiO_2$ was 2 M. This sol was used as the precursor for the subsequent deposition process.

Titanium plates of dimensions $10 \times 15 \times 1.5$ mm, provided by TIKRUTAN RT-12, Deutsche GmbH were used as substrates for the deposition. The substrates were prepared by sanding with SiC 600 paper to remove the oxide film and to achieve a uniform roughness of the deposition surface. The next step was electrophoresis of a so-prepared substrate in 5% $H_3PO_4$ solution at a voltage of 20 V for 10 min. The titanium specimens were then put inside a quarts tube in a furnace.

An ultrasonic atomizer (Gapusol 9001, RBI), using a transducer working at 1.7 MHz, was used to spray the $SiO_2$ sol. The aerosol produced entered the quartz tube (*Heraues Rof 7/50*) and at 1,000 °C was carried by air (0.07 L/s). The air velocity was approximately 1.1 cm/s, with the same average speed of aerosol drops. Films were deposited for 0.5, 1.5, 3 and 6 h at 800 °C. One of the specimens, after 6 h of deposition was kept in the quarts tube for another 4 h at 800 °C.

Finally, a layer of HA was deposited on the surface of the so-obtained thin $SiO_2$ film (deposited at 800 °C for 6 h and annealed at the same temperature for a further 4 h), by the following procedure.

An aqueous solution of stoichiometric amounts of Ca and P (Ca/P = 1.67) at a concentration of 0.065 mol/dm$^3$ was used as the precursor for the synthesis of HA the film. Concentrated nitric acid and urea (in equal molar ratio) were added to solution under vigorous stirring in order to dissolve the precipitate. The addition of thermo-hydrolysable urea was necessary in order to obtain the optimal pH in the tabular furnace.

The deposition of HA was made by wetting the surface of the thin $SiO_2$ film by very small droplets of HA aerosol, obtained using the same ultrasonic atomizer at a frequency 1.7 MHz as was used in the case of silica deposition, and by heat treatment at 800 °C for 3 h. The carrier gas was air at a flow rate of 0.07 L/s.

#### 2.1.1 *Characterization of films*

Scanning electron microscopy, SEM (JOEL 5300), equipped with a semi-automatic image analyzer (Videoplan, Kantron) was used for analyzing the morphology and homogeneity of the substrate thin films. The chemical homogeneity of the films (linear scan of Si and Ti) was analyzed on two samples. The treated elements were Si and Ti. EDS analysis was made using a Si (Bi) X-ray detector and QX 200 (Oxford Instruments, UK) connected with a scanning electron microscopy and computer multi-channel analyzer. X-rays from 0.5–20 keV with 10 eV per each channel were analyzed in the performed measurements. Semi-quantitative analysis resulted in the average ratio for both examined elements (Si and Ti) at different positions on the silica thin films. The software package ZAF (Link Company), giving good results for elements with atomic number larger than 10, was used for the estimation of the measured intensities.

The roughness and film thickness were analyzed using an ALFA STEP 500 Surface Profiler. The tip of the needle of Surface Profiler is sensitive to characteristic changes in the surface morphology. The jump of the needle between an uncovered part of the substrate (zero point) and the coated surface defines the film thickness.

The phase composition of the coatings was determined by X-ray diffractometry, XRD, (Philips PW 1050), using Cu-K$\alpha_{1\text{-}2}$ Ni-filtered radiation. The patterns were registered in the $2\theta$ ranges 9°–67° with a scanning step size of 0.02°.

Infrared spectroscopy, IR, (Perkin Elmer 983G) performed on powdered film in KBr pellets in the wave number range from 400 to 4,000 $cm^{-1}$ was also used for phase analysis.

## 3 Results and discussion

### 3.1 Mechanisms of film formation

*The SiO2 film formed after 0.5 h of deposition at 800 °C*, shown in Fig. 1a, reveals uneven parts of the deposited film, which epitaxially grew on the substrate surface. Clusters of deposited particles accumulated at the peaks of the protruding parts of the substrate, while the valley on the substrate remained uncovered. Some fully spherical particles 0.3–1 μm in diameter developed (Fig. 1a). Along the edging surface of the hills, segregated particles are interlinked by the growth of bridges. This mechanism led to the preferential growth of particles that interlink and make 'congregations'. In some areas, the concentration of the congregated forms was uniform. As a result, different spheroid and polyhedral structures were formed by the spilling over of the larger sol droplets on the protruding hills of the substrate. On these spots, deformation probably occurred and some parts of the droplets remained monolithic—mutually tightly bound; sub-droplets are visible. The surface of the film surface was very uneven and its roughness was near to the roughness of the substrate.

*$SiO_2$ film after 1.5 h of deposition at 800 °C*, shown in Fig. 1b, reveals the manner in which droplets of $SiO_2$ propagated into a vale of the substrate, depicting distribution of deposited material on the substrate hills (Fig. 1b). The fine aggregates of particles and sub-particles on the substrate surface, formed during the solidification of the sol droplets, are composed of a great number of sub-particles below 50 nm in size. These sub-particles, formed from droplets by precipitation and subsequent solidification, are organized as grape-like configurations allocated at some places and are partially knotted forming elongated polyhedral structures. Inside of the vales of the substrate, the sub-particles are intertwined forming needles, which originated from the surplus of the liquid phase flowing down the hills at the surrounding protrusions on the substrate. The partial depletion on $SiO_2$ sol occurring at the location of the vales of the substrate is conducive to the flowing of the liquid phase over a larger surface area, which, in turn, favors the formation of elongated dendrites oriented toward the bottom center of the vales. The film surface is noticeably uneven with pronounced roughness comparable with the roughness of the substrate.

*$SiO_2$ film after 3 h of deposition at 800 °C* exhibited a more uniform surface morphology. Spherical and spheroid forms of dispersed sub-parts of the aerosol droplets are shown in Fig. 1c. The uncovered parts of the substrates—partially dark patches—are not completely intertwined through the mechanism of secondary nucleation, which is mainly responsible for the filling of the deepest parts of the vales. The size of the monolithic parts of the deposit is around 1 μm and they are paired into structures of approximately 2 μm in size, which corresponds to the size of a precipitated aerosol droplet. The smallest fragments in such a unit configuration are of 30–50 nm in size. Thus, at this stage of deposition, sub-structural elements of the film are present. The aerosol droplet, which has the lowest density in its core part, undergoes uneven deformation during the process of flowing over the substrate, which in turn causes a specific morphology of these fragments of deposit, which in form resemble pits made by etching.

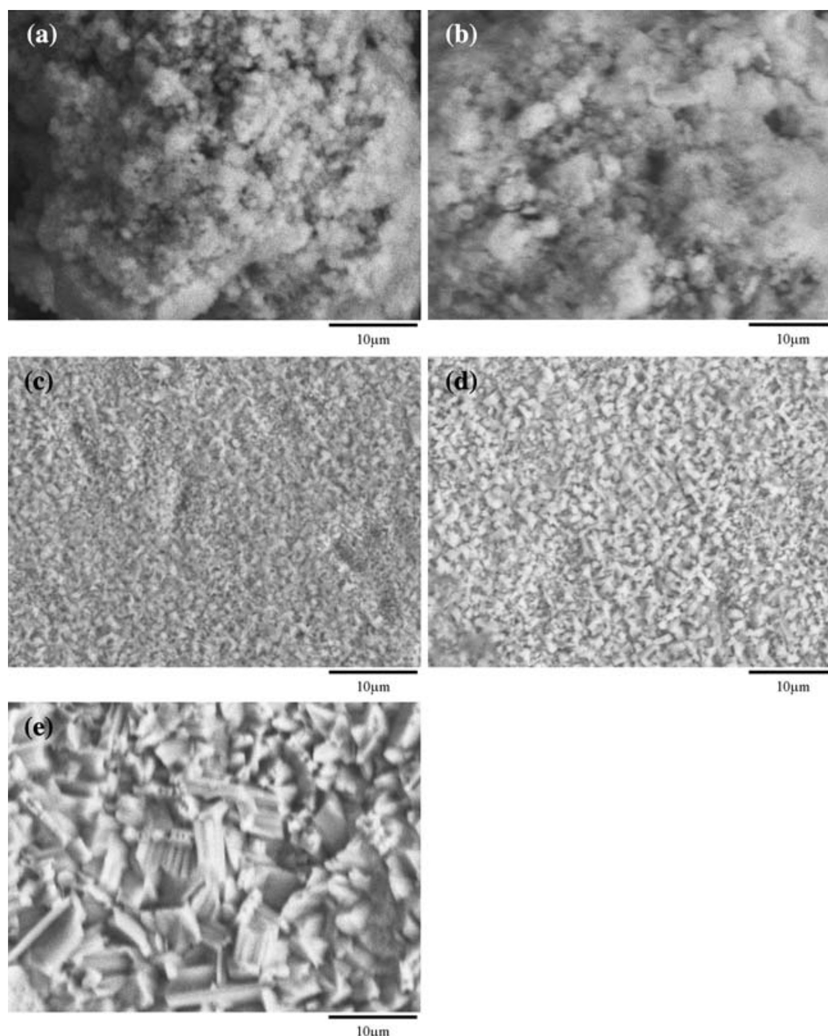


**Fig. 1** Typical SEM appearance of $SiO_2$ films obtained at 800 °C after different deposition time; 0.5 h (**a**), 1.5 h (**b**), 3 h (**c**), 6 h (**d**), and 6 h + 4 h annealing (**e**)

*The $SiO_2$ film formed after 6 h of deposition at 800 °C* has the morphology of elongated grains formed by polygonization of intertwined smaller oval grains (Fig. 1d). The grains are mainly of cubic or parallelepiped shape, where the latter was achieved by connecting cubic-form grains. The poligonization and connecting proceeded by a sintering process during the long residence time of the substrate/film system in the furnace. The film texture is a mixture of these two dominant grain shapes of 1 μm and 2 μm in size.

*The $SiO_2$ film formed after 6 h of deposition and 4 h of annealing at 800 °C* shown in Fig. 1e reveals a fully homogeneous film over the whole substrate. In this case, the former grains dominantly of spheroid shape gradually transformed into a net of polyhedral grains of approximately same size (the grain size is mainly determined by the size of the aerosol drops).

After a sufficiently long holding time at the furnace temperature (6 h of deposition and 4 h of annealing), it is apparent that the $SiO_2$ grains had grown considerably. The growth was achieved by the "coagulation" of smaller grains by creating small-angled polyhedral grains/subgrains with different aspect ratios. Most frequently, the grains are more or less elongated and were made by the sintering of fragments of already-formed grains alongside one of the plane of the existing polyhedral form—a road-shaped grain (Fig. 1d).

The topography of the film surface is caused by the original non-homogeneity of the density of the film, which was caused by the unevenness of the substrate roughness. Also, as the sintering process was in the final stage, it is probably that the obtained density of the film was greater and the average radius of the grains increased as the result of sintering during the annealing process.

## 3.2 Thickness and roughness

The thickness, average and maximal roughness of films on titanium substrate obtained after different deposition (and annealing) times are given in Table 1.

**Table 1** The thickness and roughness of thin $SiO_2$ films deposited at 800 °C for various deposition times

| Sample | Deposition time, h | Film thickness, µm | Average roughness, µm | Max roughness, µm |
|---|---|---|---|---|
| 1 | 0.5 | – | – | – |
| 2 | 1.5 | 3 | 12 | 20 |
| 3 | 3 | 8 | 8 | 12 |
| 4 | 6 | 19 | 3 | 5 |
| 5 | 6 + 4* | 15 | 5 | 8 |

4*-Annealing time at 800 °C

After 1.5 h of deposition, the $SiO_2$ film had almost completely covered the surface of the substrate. After 3 h, the film had gained its essential thickness, the substrate was fully covered and the average and maximum roughness were considerably lower than those for the film deposited for only 1.5 h, and they were 8 and 12 µm, respectively. After 6 h of deposition, the film thickness had increased to 19 µm, while the average roughness was reduced to 3 µm, while the maximum roughness was 5 µm.

Additional annealing (for 4 h at 800 °C) of the sample deposited during 6 h increased the roughness of the film (5 µm average roughness and 8 µm maximum roughness) and decreased the film thickness to 15 µm. The observed changes in roughness and thickness were produced through densification achieved by sintering, whereby the densities of different films fragments deposited on parts of the titanium substrate with different roughness.

The regions belonging to vales of the substrate which were 'bridged' through a secondary nucleation process had significantly lower density than other parts of the coating. Therefore, during annealing, the process of diffusion along the grain boundaries resulted in low-density regions being filled, causing visible changes in the surface morphology of the coating, i.e., increased roughness and decreased thickness.

## 3.3 Homogeneity of film composition

The results of the EMPA analysis for Si and Ti in the deposited films are presented in Table 2.

Films deposited for a short time (0.5 and 1.5 h) showed the presence of significant amounts of Ti, the source of which was the titanium substrate. In the case of samples deposited for only 0.5 h, Ti is the principle constituent because the deposited silicon dioxide was very unevenly spread and very thin. Therefore, it is likely that, together with Ti atoms from the bare—uncovered—titanium substrate, Ti atoms beneath the very thin films also contribute to the total collected signals from the scanned films surfaces.

Depending on the area scanned, the concentration of silicon varied from 14.7 to 30.2 wt%, while the concentration of Ti fluctuated from 69.8 to 85.3 wt%. These results show that during this stage of deposition, the process of secondary nucleation of $SiO_2$ had not yet started and that the process of the formation of isolated islands of film was the dominant process of the film integration.

**Table 2** EPMA analysis for Si and Ti in deposited $SiO_2$ thin films

| Sample | Deposition time, h | Location | Chemical somposition, mass% | |
|---|---|---|---|---|
| | | | Ti | Si |
| 1 | 0.5 | 1 | 81.2 | 18.8 |
| | | 2 | 78.1 | 21.9 |
| | | 3 | 74.3 | 25.7 |
| | | 4 | 69.8 | 30.2 |
| | | 5 | 73.4 | 26.6 |
| | | 6 | 85.3 | 14.7 |
| 2 | 1.5 | 1 | 17.2 | 82.8 |
| | | 2 | 18.1 | 81.9 |
| | | 3 | 21.3 | 78.7 |
| | | 4 | 13.9 | 86.1 |
| | | 5 | 14.5 | 85.5 |
| | | 6 | 22.9 | 77.1 |
| | | 7 | 16.1 | 83.9 |

In the samples that had undergone 1.5 h of deposition, the Ti concentration were 13.9 to 22.9 wt% and the Si concentration varied from 77.1 to 86.1 wt%, which implies the $SiO_2$ film mainly covered the surface. However, this result also shows that the process of secondary nucleation in bridging the vales of the titanium substrate was not yet completed.

After 3 h of deposition, there were no more signals of Ti in the film, meaning that the substrate was fully covered by a $SiO_2$ film. Secondary nucleation and the process of the 'filling-up' of the vales of the substrate surface were completed so that further deposition proceeds evenly on the whole deposition surface.

## 3.4 Phase analysis of the $SiO_2$ film

### *3.4.1 X-ray diffraction*

X-ray diffraction diagram in Fig. 2 shows that regardless of the deposition time and the additional annealing process (of 4 h duration) the phase of the deposited film remained amorphous $SiO_2$.

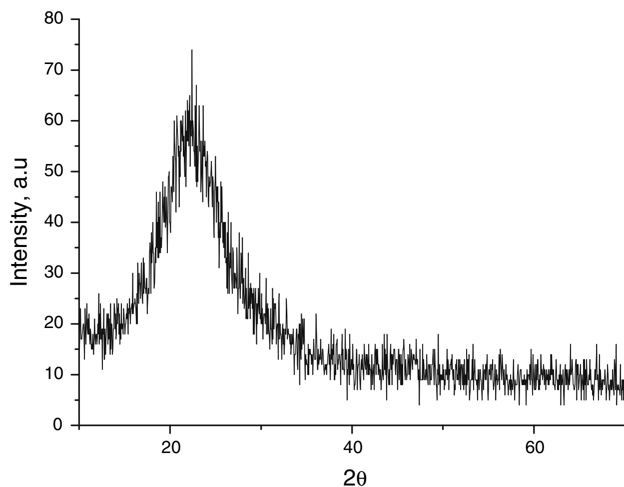


**Fig. 2** XRD diffraction of $SiO_2$ film deposited at 800 °C

### *3.4.2 Infra red spectroscopy*

The IR spectra of specimens of SiO2 film pealed off from all the deposited samples are very similar. The characteristic transmittance bands from $SiO_2$ deposited for 0.5 h correspond to the following wave numbers: 3,394 $cm^{-1}$; 1,573 $cm^{-1}$; 1,369 $cm^{-1}$; 1,034 $cm^{-1}$; 746 $cm^{-1}$; and 414 $cm^{-1}$ (Fig. 3a–e.). These energies correspond to the characteristic vibrations of different molecular groups belonging to the silicon dioxide system [29–32].

The band at 3,394 $cm^{-1}$ corresponds to the stretching vibration mode of silanol groups (Si-OH) and adsorbed water. The band at 1,573 $cm^{-1}$ relates to the bending vibration of the OH group of molecular water. This band is slightly shifted from the value of 1,628 $cm^{-1}$ reported in the literature as the ideal.

The band at 1,034 $cm^{-1}$ corresponds to the transversal asymmetric vibrations of Si-O-Si. The shifting of this value towards lower value of wave number indicates the movement of O atom alongside the line parallel to the Si–Si axes. In turn, this causes a distortion in the surrounding Si–O bonds, bringing about a so-called asymmetric transversal oscillation causing the cationic shifting.

The band at 746 $cm^{-1}$ corresponds to the rocking deformation in the Si–O–Si chains created by the coupling of the transversal symmetric vibration of O atom alongside the bisection of Si–O–Si angles, with the simultaneous movement of Si cations (3a–e).

The band at 414 $cm^{-1}$ arises from the transversal optic rocking mode of Si–O–Si, created by the stretching vibrations of O atom regarding the position of the Si atom in Si–O–Si chain [29–32].

In case of $SiO_2$ deposited by spray pyrolysis during 1.5 h, the band corresponding to the stretching vibration of silanol groups has the minimum for the value of the wave number of 3,382 $cm^{-1}$ (Fig. 3b).

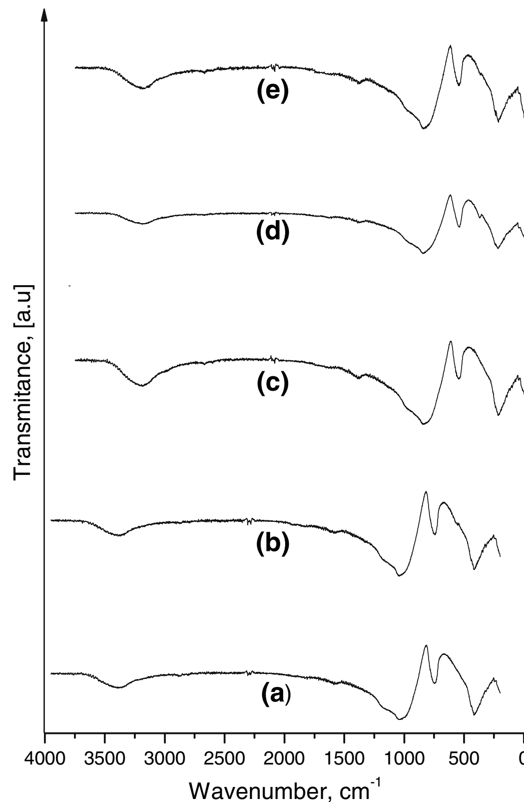


**Fig. 3** IR spectra of $SiO_2$ thin films after deposition for (**a**) 0.5 h, (**b**) 1.5 h, (**c**) 3 h, (**d**) 6 h and (**e**) 6 h + 4 $h_{annealing}$

The band at 1,573 $cm^{-1}$ is shifted at the value of 1,583 $cm^{-1}$. For $SiO_2$ deposited during 3 h, a small shift to the value at 409 $cm^{-1}$ was recorded for the band which corresponds to wave number of 414 $cm^{-1}$ (Fig. 3c).

After 3 h and 6 h of deposition, and 6 h of deposition with subsequent annealing during the 4 h, all above recorded bands are shifted by approximately 200 $cm^{-1}$ in the direction of smaller wave numbers (Fig. 3d). The band at 3,394 $cm^{-1}$ for $SiO_2$ deposited during 0.5 and 1.5 h was shifted to 3,188 $cm^{-1}$ after at 3 h, 3,178 $cm^{-1}$ after 6 h and to 3,183 $cm^{-1}$ after 6 h of deposition and 4 h of annealing. The band at 1,034 $cm^{-1}$ was shifted to 829 $cm^{-1}$ after 3 h, 840 $cm^{-1}$ after 6 h and 834 $cm^{-1}$ after 6 h of deposition and 4 h of annealing. The band at 746 $cm^{-1}$ was shifted 541 $cm^{-1}$ after 3 h and to 542 $cm^{-1}$ for $SiO_2$ deposited after 6 h with and without subsequent annealing for 4 h. The band at 414 $cm^{-1}$ shifts to 214 $cm^{-1}$ after 3 h and to 211 $cm^{-1}$ after 6 h of deposition both with and without annealing for 4 h (Fig. 3e).

It is apparent that significant shifting of the IR bands in the deposited $SiO_2$ occurred between the samples deposited for 1.5 and 3 h. During this deposition period (from 1.5 to

3 h) intensive movement of the atoms occurred, leading to their consolidation inside the silicon dioxide tetrahedral structure. The straightforward consequence of the occurred rearrangement of the atoms in the deposited $SiO_2$ is the shifting of all characteristic vibrations toward smaller wave numbers (larger energies), while the shapes of all these bands remains almost unchanged, which in turn implies that only the shifting of the characteristic vibrations towards the higher energies is encountered.

## 3.5 HA thin films on the surface of $SiO_2$ films

### *3.5.1 Morphology and thickness of the HA films*

After 3 h of deposition HA, the surface of the $SiO_2$ thin film (thin $SiO_2$ film obtained after 6 h deposition and 4 h of annealing at 800 °C) was completely covered with calcium hydroxyapatite, as can be seen from Fig. 4. The particles of calcium hydroxyapatite were mostly of submicron dimensions (0.5–1 μm). The particles have different morphologies, polygonal, rounded and needle-shaped. The majority are needle-shaped joined together forming "flowers" like structures with diameters smaller than 0.1 μm. The measured average thickness of the so-obtained HA film determined using the surface profiler method was around 3 μm. The particles agglomerated into large blocks of the previous formed layers of the thin film during spray pyrolysis. In Fig. 4, they are shown preferently as grey spots and the flower or petal-like structures belong to the newly formed layers (with a smaller film density inside them) are shown as white spots.

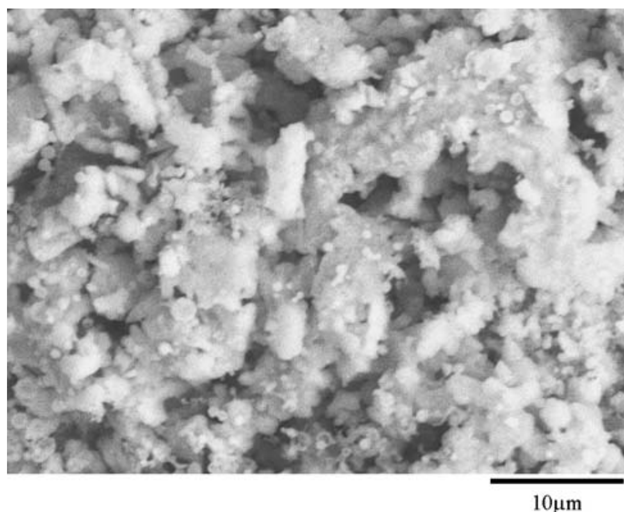


**Fig. 4** Microstructure of a hydroxyapatite thin film after deposition on a $SiO_2$ film for 3 h

### *3.5.2 Phase composition of HA thin films*

Phase analysis of the thin HA films was performed by XRD spectroscopy. The XRD patterns in Fig. 5 show all the characteristics peaks for calcium hydroxyapatite, corresponding to literature data (JCPDS No.9-432).

The IR spectrum in Fig. 6 shows all the characteristic bands for hydroxyapatite [10, 24, 25]. The asymmetrical stretching ($v_3$) and bending ($v_4$) modes of $PO_4^{3-}$ ions were detected at around 1,092 and 1,042, and 603 and 569 $cm^{-1}$, respectively. The symmetrical stretching modes ($v_1$ and $v_2$) of $PO4^{3-}$ ions were found at around 957 and 473 $cm^{-1}$. The liberation and stretching mode of $OH^-$ ions were detected at around 630 $cm^{-1}$and 1,626 $cm^{-1}$, respectively. The stretching vibrations ascribed to $CO_3^{2-}$ at around 1,442, 1,406 and 875 $cm^{-1}$ are also present. This indicates that

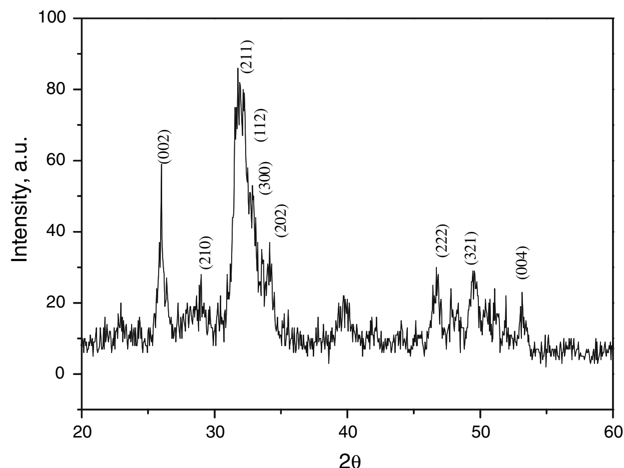


**Fig. 5** X-ray diffraction pattern of hydroxyapatite thin film on surface of $SiO_2$ film

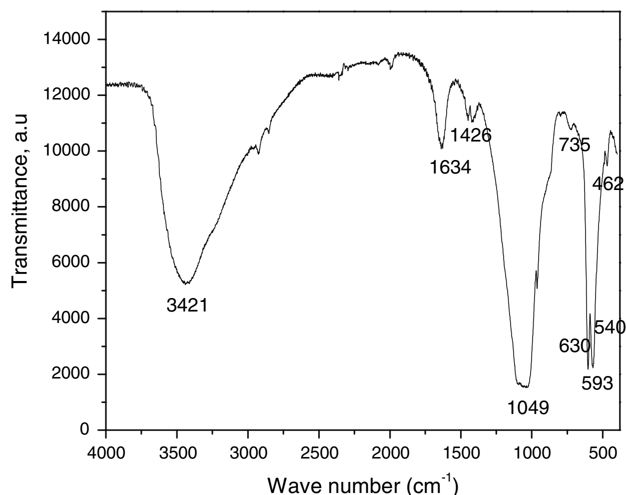


**Fig. 6** IR spectra of a hydroxyapatite thin film on the surface of a $SiO_2$ film

carbonate groups are incorporated into the apatite structure. The band registered at 630 $cm^{-1}$ belongs to the liberation mode of the $OH^-$ vibration.

#### 3.5.3 Possible mechanisms of formation of calcium hydroxyapatite on a $SiO_2$ coating

Texture and chemical activity of deposited $SiO_2$ film is critically dependent on its nano-structural design conducive for an increased surface activity, which is important for the formation bonds of appropriate strength between the thin $SiO_2$ film and the hydroxyapatite deposited on its surface.

The mechanism of formation of calcium hydroxyapatite on the surface of a $SiO_2$ film, most probably, goes through the formation of a hydrate layer of $SiO_{2-x}OH_x$ on the surface of $SiO_2$ film in the first stage of the growth of the hydroxyapatite on the film. On such a surface layer, deposition of $Ca^{2+}$ and $PO_4^{3-}$ ions proceeds by one of two possible mechanisms: (i) calcium and phosphate ions of the HA sol in contact with $SiO_{2-x}OH_x$ should more readily precipitate forming hydroxyapatite or/and (ii) the surface of $SiO_{2-x}OH_x$ may attract $Ca^{2+}$ ions and combine phosphate ions in $SiO_{2-x}OH_xHPO_4$ by covalent bonding and forming apatite in a similar way [8, 23, 26–28].

## 4 Conclusion

This paper presents a method for the deposition of thin $SiO_2$ film by ultrasound wet spray pyrolysis of a silica sol. The precursor solution for the sol is a very narrow size distribution of $SiO_2$ particles obtained by hydrothermal precipitation of silicon acid.

The mechanism of the deposition of the films, the change of their morphology and the chemical homogeneity of deposits are considered for different times of deposition. Particular attention was given to the thickness and roughness of the films. It was shown that the entire surface had been covered with a film of thickness sufficient to preclude any secondary excitation of the titanium substrate (no signal from titanium was detected) after 3 h of deposition at 800 °C.

After 6 h of deposition, the roughness of the deposited film had considerably decreased to a value of 5 μm, while the thickness of the film was of maximal value of 19 μm. After an additional 4 h of annealing of this film, the thickness of the film decreased down to 15 μm while the average roughness increased to 8 μm. It was estimated that this sufficiently long deposition time in addition to 4 h of annealing causes a considerable grain coarsening, attained by association of smaller grains into larger ones, wherein the polyhedral structure with different length/diameter ratios are generated.

Sometimes these grains have a plate-like shape while other times they exhibit a preferential one-directional growth and have a road-like shape. The outlined morphology of the film is conducive for the deposition of hydroxyapatite due to the high concentration of defects within its fine roughness and the innate fine nano-structure of the film.

The thin HA film deposited on the surface of the thin $SiO_2$ film was completely continuous with a prevailing needle-shaped morphology. Its phase composition corresponded to hydroxyapatite and had a thickness of approximately 3 μm.

**Acknowledgments** This research was supported by the INCOMAT NMP3-CT-2007-032918 by the grant 0329178, and Ministry of Science and Environmental Protection of the Republic of Serbia by the grant 142066.

## References

1. G. L. MESSING, S. C. ZHANG, G. V. JAYANATHY, *J. Am. Ceram. Soc.* **76** (1993) 2707
2. G. V. JAYANATHY, S. C. ZHANG, G. L. MESSING, *J. Aerosol Sci. Technol.* **19**, (1993), 478
3. K.OKUYAMA, W. L. LENGERO, *Chem. Eng. Sci.* **58** (2003), 537
4. F. ISKANDAR, I. W. LENGERO, B. XIA, K. OKUYAMA, *Nanoparticle Res.* **3**, (2001), 263
5. F. I. MIKRAJUDDIN, F. ISKANDAR, K. OKUYAMA, *Nano Lett.* **1** (2001), 231
6. V. JOKANOVIĆ, in “Finely Dispersed Particles:Micro-, Nano- and Atto-Engineering” (CRC, Taylor and Francis, New York, 2005)
7. V. JOKANOVIĆ, B. JOKANOVIĆ, *Am. Cer. Soc. Bull.* **85** (2006) 26
8. V. JOKANOVIĆ, D. USKOKOVIĆ, *Mat. Trans., JIM* **46** (2005) 228
9. V. JOKANOVIĆ, Dj. JANAĆKOVIĆ, D. USKOKOVIĆ, *Ultrason. Sonochem.* **6** (1999) 1570
10. V. JOKANOVIĆ, I. NIKČEVIĆ, B. DAČIĆ, D. USKOKOVIĆ, *J. Cer. Process. Res.* **5** (2004) 157
11. A. STOCH, A. BROEK, G. KMITA, J. STOCH, W. JASTRZBSKI, A. RAKOWSKA, *J. Mol. Struct.* **596** (2001) 191
12. L. G. YU, K. A. KHOR, H. LI, P. CHEANG, *Biomaterials* **24** (2003) 2695
13. L. IN-SEOP, P. JONG-CHUL, L. YOUNG-HEE, *Surf. Coat. Technol.* **171** (2002) 252
14. G. BIKULIUS, V. BIROKAS, A. MARTUIEN, E. MATULIONIS, *Sur. Coat. Techn.* **172** (2003) 139
15. I. S. LEE, C. N. WHANG, G. H. LEE, F. C. CUI, A. ITO, *Nucl. Instr. Meth. Phys. Res. Sec.* **179** (2001) 364
16. J. L. ARIAS, M. B. MAYOR, J. POU, Y. LENG, B. LEON, M. PEREZ-AMOR, *Biomaterials* **24** (2003) 3403
17. H. MING-FA, P. LI-HISIANG, C. TSUNG-SHUNE, *Mater. Chem. Phys.* **74** (2002) 245
18. V. JOKANOVIĆ, M. D. DRAMIĆANIN, Ž. ANDRIĆ, B. JOKANOVIĆ, Z. NEDIĆ, A. M. SPASIĆ, *J. All. Comp.* (2007) In press (doi: 10.1016/j.jallcom.2006.11.151)

19. V. JOKANOVIĆ, M. D. DRAMIĆANIN, Ž. ANDRIĆ, T. DRAMIĆANIN, M. PLAVŠIĆ, M. MILJKOVIĆ, *Opt. Mat.* (2007) In press (doi: 10.1016/j.optmat.2007.05.043)
20. D. MARKOVIĆ, V. ŽIVOJINOVIĆ, V. JOKANOVIĆ, V. KRSTIĆ, *Acta Veterinaria* **56** (2006) 541
21. R.Z. GEROS, in “Calcium phosphates in oral biology and medicine” (New York University, College of Dentistry, 1991), p. 114
22. G. C. ENGELMAYER, E. RABKIN, F. W. H. SUTHERLAND, F. J. SCHOEN, J. E. MAYER, M. M. SAKS, *Biomaterials* **26** (2005) 175
23. H. M. KIM, F. MIYAJI, T. KOKUBO, T. NAKAMURA, *J. Biomed. Mater. Res.* **38** (1997) 121
24. B. FENG, J. Y. CHEN, S. K. QUI, L. HE, J. Z. ZHAO, X. D. ZHANG, *Biomaterials* **23** (2002) 505
25. I. NIKCEVIC, V. JOKANOVIC, M. MITRIC, Z. NEDIC, D. MAKOVEC, D. USKOKOVIC, *J. Sol. St. Chem.* **177** (2004) 2565
26. V. JOKANOVIC, D. IZVONAR, M. D. DRAMICANIN, B. JOKANOVIC, V. ZIVOJINOVIC, D. MARKOVIC, B. DACIC, *J. Mater. Sci: Mater. Med.* **17** (2006) 539
27. Y. XIAOXIA, H. XIAOHUI, Y. CHENGZHONG, D. HEXIANG, W. YI, Z. ZHENDONG, Q. SHIZHANG, L. GAOQING, Z. DONGYUAN, *Biomaterials* **27** (2006) 3396
28. C. G. L. SANDER, G. C. W. JOOP, C. S. MARIJKE, S. JOOP, A. J. JOHN, *Biomaterials* **27** (2006) 3368
29. C. V. RAGEL, M. VALLET-REGEL, L. M. RODRIGUEZ-LORENZO, *Biomaterials* **23** (2002) 1865
30. E. MATIJEVIC, *Chem. Mater.* **5** (1993) 412
31. A. VAN BLAADEN, A. VRIJ, *Langmuir* **8** (1992) 2921
32. H. ZHU, Y. MA, Y. FAN, J. SHEN, *Thin Sol. Films* **397** (2001) 95